

## Article

# Ultrasonication Assisted Catalytic Transesterification of Ceiba Pentandra (Kapok) Oil Derived Biodiesel Using Immobilized Iron Nanoparticles

Mithileth Pasawan <sup>1,\*</sup>, Shiao-Shing Chen <sup>1,\*</sup>, Bhanupriya Das <sup>2</sup>, Hau-Ming Chang <sup>1</sup>, Chang-Tang Chang <sup>3</sup>, Thi Xuan Quynh Nguyen <sup>1</sup>, Hong-Ming Ku <sup>4,\*</sup> and Yue-Fang Chen <sup>5,\*</sup>

<sup>1</sup> Institute of Environmental Engineering and Management, National Taipei University of Technology, Taipei 10608, Taiwan; mithileshpaswan037@gmail.com (M.P.); whowindow@gmail.com (H.-M.C.); xuanquynhaby@gmail.com (T.X.Q.N.)

<sup>2</sup> Department of Chemical Engineering, Indian Institute of Technology Guwahati, Guwahati 781039, India; bhanupriyadas786@gmail.com

<sup>3</sup> Department of Environmental Engineering, National I-Lan University, Yilan 24670, Taiwan; ctchang@niu.edu.tw

<sup>4</sup> Department of Chemical Engineering Practice School, King Mongkut's University of Technology Thonburi, Bangkok 10140, Thailand

<sup>5</sup> School of Energy and Environmental Engineering, University of Science and Technology Beijing, Beijing 100083, China

\* Correspondence: f10919@ntut.edu.tw (S.-S.C.); hongming.ku@gmail.com (H.-M.K.); chen Yuefang@ustb.edu.cn (Y.-F.C.)



**Citation:** Pasawan, M.; Chen, S.-S.; Das, B.; Chang, H.-M.; Chang, C.-T.; Nguyen, T.X.Q.; Ku, H.-M.; Chen, Y.-F. Ultrasonication Assisted Catalytic Transesterification of Ceiba Pentandra (Kapok) Oil Derived Biodiesel Using Immobilized Iron Nanoparticles. *Fuels* **2022**, *3*, 113–131. <https://doi.org/10.3390/fuels3010008>

Academic Editor: Maria A. Goula

Received: 24 December 2021

Accepted: 9 February 2022

Published: 22 February 2022

**Publisher's Note:** MDPI stays neutral with regard to jurisdictional claims in published maps and institutional affiliations.



**Copyright:** © 2022 by the authors. Licensee MDPI, Basel, Switzerland. This article is an open access article distributed under the terms and conditions of the Creative Commons Attribution (CC BY) license (<https://creativecommons.org/licenses/by/4.0/>).

**Abstract:** The embedded immobilized enzymes (*Rhizopus-oryzae*) on the magnetic nanoparticles (Fe<sub>3</sub>O<sub>4</sub>-NPs) is a new application for the sustainable production of high-quality biodiesel. In this study, biodiesel is derived from Kapok oil via ultrasonication (US)-assisted catalytic transesterification method. A novel attempt is made to prepare magnetic nanoparticles embedded by an immobilized enzyme to solve the problem of enzyme denaturation. This innovative method resulted in optimum biodiesel conversion of 89 ± 1.17% under reactant molar ratio (methanol: oil) of 6:1, catalyst loading 10 wt% with a reaction time of 4 h at 60 °C. The kinetic and thermal study reveals that conversion of Kapok oil to biodiesel follows a pseudo first-order reaction kinetic with a lower ΔE of 30.79 kJ mol<sup>-1</sup>. The ΔH was found to be 28.06 kJ mol<sup>-1</sup> with a corresponding ΔS of -237.12 J mol<sup>-1</sup> K<sup>-1</sup> for Fatty Acid Methyl Ester formation. The ΔG was calculated to be from 102.28 to 109.40 kJ mol<sup>-1</sup> for temperature from 313 K to 343 K. The positive value of ΔH and ΔG is an indication of endothermic and non-spontaneous reaction. A negative ΔS indicates the reactant in the transition state possesses a higher degree of ordered geometry than in its ground state. The immobilized catalysts provided great advantages towards product separation and efficient biodiesel production. **Highlights:** 1. Effective catalytic transesterification assisted by the ultrasonication method was used for bi-odiesel production. 2. Magnetite nanoparticles synthesized by the co-precipitation method were used as heterogeneous catalysts. 3. An immobilized enzyme (*Rhizopus-oryzae*) was embedded in the heterogeneous catalyst, as it is reusable and cost-effective. 4. The maximum biodiesel yield obtained from Kapok oil was 93 ± 1.04% by catalytic trans-esterification reactions.

**Keywords:** Kapok oil; transesterification; biodiesel; immobilized magnetite catalysts; kinetic and thermodynamic analysis

## 1. Introduction

The economically significant production of carbon-neutral biodiesel from non-edible oilseeds has attracted attention as the ultimate alternative to depleting resources of petrodiesel [1]. The economic yet sustainable production of biodiesel from non-edible oilseeds as feedstock has caught the attention as a promising alternative to conventional diesel due to

its renewable and environmentally friendly nature [2,3]. In the wake of the issues concerning the increased demand for edible vegetable oil, environmentalists are concerned about a negative impact on the food chain due to biodiesel production. Consequently, researchers have focused on non-agro based feedstock that is abundant such as Mahua, Jojoba, Jatropha and microalgae as a major source to derive biodiesel [3–6]. Unlike edible oil seeds that provide tough competition to using the land for production as the feedstock of biodiesel, these non-edible oil plants grow in wastelands, which further aids as green cover to the wastelands [7]. Besides, the decentralized nature of such a renewable energy technology makes it well suited to the rural context [4,8]. In this regard, *Ceiba pentandra*, a non-edible oilseed locally known as kapok, can be used as raw material for producing biodiesel of high quality. It is mainly composed of cellulose, lignin, polysaccharide, and a small amount of waxy coating to give it more hydrophobic characteristics [5]. In addition, the kapok seed oil is relatively cheaper than other feedstocks and has good oxidation stability with a saturated fatty acid of 71.95%, which is higher than that of coconut oil [6,8]. However, the application and natural production of this non-edible oilseed remain underutilized. The most common process to synthesize biodiesel also known as Fatty Acid Methyl Ester (FAME), is by transesterification in presence of an alkaline, acidic, or enzymatic catalyst. A previous study reported that kapok oil-derived biodiesel via transesterification had properties that complied with the ASTM standard [5]. Over the past several years, a new technology called enzyme-catalyzed transesterification assisted by ultrasonication has been utilized to optimize the yield of biodiesel. The major advantage of ultrasonication is the capability to remove the mass transfer limitation in the transesterification reaction [9], and ultrasonication in the emulsification of the immiscible liquids reactants during biodiesel production leads to the generation of microturbulence by a radial motion of cavitation bubbles that affects the surface of the catalysts and generates a new active surface of the catalysts. Hence, it is more suitable for producing biodiesel than magnetic or mechanically stirring [10–13].

Furthermore, enzymatic transesterification using ultrasonication demonstrated not only enhancement in catalytic activity but also stability of the enzyme. Besides, enhancing the longevity of enzyme biocatalysts with optimized reaction time, reaction temperature, and less power consumption make the process profitable [12,14–16]. From jatropha oilseed using  $\text{Al}_2\text{O}_3/\text{CH}_3\text{OH}$ , the conversion achieved was 84% with methanol /oil mole ratio of 12:1, reaction time 4 h, and 6 wt% catalysts under 70 °C [17]. Cooking oil with the immobilized enzyme (Novozym 435) under ultrasound irradiation achieved the FAME conversion of 86.6% at 4 h [18]. Ethanol to soybean oil with a molar ratio of 3:1 at 70 °C using 20 wt% of Novozym 435 was reported to achieve 88% FAME production after 240 min. Ethanol to macauba oil molar ratio 9:1 at 65 °C with 20 wt% loading of Novozym 435 to 70% conversion of Macauba oil was obtained after 90 min [19]. Kumar et al. (2018) reported biodiesel production employing ultrasound-assisted transesterification using  $\text{Na}/\text{SiO}_2$  as a catalyst. The ultrasonic irradiation of 50% amplitude at 0.7 cycle/second boosted the rate of reaction with a biodiesel yield of more than 98% [20]. Also, the reaction time was reduced to 90 s in comparison to a conventional processing time of 6 h. Overall, the process provided simplicity in handling as the low-cost instruments were able to produce high yields with catalyst regeneration. Although enzyme-based reactions consume less energy, are more environmentally friendly, and do not promote side reactions, they are expensive and their regeneration from the reaction mixture is difficult [21,22]. Therefore, an enzyme-catalyzed process alone is not an economical process at the industrial level, and immobilized-lipases-mediated transesterification seems to be a favorable option in the future. Lipase in its free form is difficult to reuse and comparatively costly to the alkali catalyst [23,24]. On the other hand, an immobilized lipase is reusable and flexible to various engineering designs. Studies were conducted on the effect of two lipases in their immobilized forms at 40 °C and methanol to oil ratio (6:1). The conversion was dependent on the type of lipase species [25,26].

Embedding immobilized enzyme on the magnetic nanoparticles is a bio-nanocatalyst and a new application for the production of biodiesel from different feedstocks. Previous studies report the use of silica, iron, polymeric nanoparticles for lipase immobilization [27–29]. However, nanoscale magnetite ( $\text{Fe}_3\text{O}_4$ ) has an edge over the others when used as support for enzyme immobilization since it favors the separation of immobilized enzymes and enhanced stability with good binding efficiency, large surface area, low mass transfer resistance and less fouling. In addition, it demonstrates super-paramagnetic properties with good biocompatibility [30]. To the best of our knowledge, the production of kapok oil-derived biodiesel with catalyst has not been reported yet. In this paper, we discuss the outcomes of experiments to achieve maximum extraction of kapok oil-based biodiesel and magnetite nanoparticles as the catalysts synthesized by the co-precipitation method to initiate the esterification reaction under the influence of ultrasound irradiation by the immobilized enzyme (*Rhizopus-oryzae*) for making biodiesel. The fuel properties were determined by ASTM D6751 standard methods [5]. The compositional analysis of synthesized biodiesel was characterized by their hydrocarbon group using Gas Chromatography-Mass Spectrometry analysis (GC-MS). To confirm the presence of the volatile functional compounds, Fourier Transform Infrared Spectroscopy analysis (FTIR) was used. Besides, real-time monitoring of the course of the transesterification reaction with the corresponding chemical shift of hydroxylic protons of glycerol in the ester-rich phase and methanol was carried out using Proton Nuclear Magnetic Resonance ( $^1\text{H}$  NMR). Furthermore, kinetics and thermodynamic aspects of the production of Kapok oil-derived biodiesel with catalyst were also reported in this study.

## 2. Experimental Setup

### 2.1. Materials

Kapok seeds were obtained from Guwahati, India, and *Rhizopus-oryzae* enzyme was obtained from the Institute of Microbial Technology, Chandigarh, India. Methanol, sodium hydroxide, iron chloride, potassium iodide, ammonia solution, glycerol and methanol were procured from Sigma-Aldrich Co., Ltd. (Burlington, MA, USA). All chemicals used are of analytical grade.

### 2.2. Procedure for Synthesis of Magnetite Nanoparticles

A 12.97% (*w/v*) iron (III) salt aqueous solution was prepared by anhydrous ferric chloride ( $\text{FeCl}_3$ ) dissolved in distilled water and 13.17% (*w/v*) of potassium iodide (KI), also dissolved in distilled water to prepare an aqueous solution of potassium iodide. Further, the prepared potassium iodide solution was mixed with iron (III) salt solution in a 3:1 ratio at ambient temperature. Continuous stirring was applied for an hour to achieve equilibrium. After that, filtration of precipitated iodine was carried out, followed by distilled water wash and drying at 100 °C and finally weighed. The yield was 86.6%. The whole volume of the filtration was hydrolyzed using ammonia ( $\text{NH}_3$ ) solution (25%). Drop-wise addition of solution was carried out with constant stirring until the black magnetite (pH 10) precipitated completely. The magnetite nanoparticles that were obtained were filtered, and this was followed by washing with distilled water and drying at 250 °C. It was then weighed to achieve a yield of iron salts of 99% [29,31].

### 2.3. Immobilization of *Rhizopus-Oryzae* Enzyme on Iron Nanoparticles

Magnetite nanoparticles were dispersed in 99.9% ethanol solution and then decanted by the magnetic device. Immobilization of lipase was then accomplished by using a 1 mL carrier, 1 mg of *Rhizopus-oryzae* enzyme, 2.5 mg of decanted magnetite nanoparticles, and buffered by 0.5 mL phosphate salt (pH 6.5). The mixture was incubated at 4 °C for 12 h at 30 rpm. Thereafter, the mixture was kept for stirring at 5000 rpm for 5 min to remove the insoluble part from the mixture. It was then washed with buffer to get rid of the unbound proteins. Bradford's technique was utilized to determine the concentration of proteins in

the solution. Finally, an immobilized catalyst (lipase-MNPs) was stored at 4 °C for further application [32,33].

#### 2.4. Oil Extraction from the Kapok Oilseeds

The seeds are dried in sunlight for two to three days to remove moisture. After that, the seeds are crushed, oven-dried at a temperature of 105 °C to eliminate any traces of moisture [34]. Thereafter, the dried kapok seeds are weighed to 10 grams and positioned on a thimble, which was placed into the Soxhlet apparatus. Petroleum benzene is used as a solvent in this experiment with a solvent to seed ratio of 17.5% (*v/w*). It is then poured into a three-necked round bottom flask connected with the extractor and joined by a condenser on top to avoid any solvent losses. A temperature controller heater is used to maintain the temperature in the apparatus. A thermometer is inserted in one of the necks of the flask to measure the temperature, and 8 hours later, the process is stopped. The oil trapped in the solvent is then separated using a rotary evaporator under vacuum pressure at 65 °C. This extracted oil after evaporation is found to be 2.3 g by mass, while the yield of kapok oil according to Equation (1) is calculated to be 23%.

$$\text{Yield (\%)} = \frac{\text{Mass of extracted oil}}{\text{Mass of seed fed}} \times 100 \quad (1)$$

#### 2.5. Physiochemical Properties of Kapok Oil

Physiochemical properties are performed to analyze the quality of the feedstock and are presented in Table 1. In this experiment, 2 g of kapok oil has been taken in a conical flask with 20 mL of neutralized alcohol solution and then kept for mixing using a magnetic stirrer. The mixed solution was heated for 10 min followed by the addition of a few drops of phenolphthalein indicator. The mixed solution is then put for titration against potassium hydroxide solution (0.1 N) with a KOH volume of 6.621 mL. The appearance of a pink color indicated the endpoint, then calculated the acid value and Free fatty acid (FFA) content. On the other hand, 1 g of kapok oil was poured into a tared beaker. It was then dissolved in 3 mL of ethanol. To the mixture, 25 mL, KOH of strength 0.5 N was added and stirred well before being attached to the reflux condenser. An additional reflux condenser was considered for the blank sample with the rest of the reagents present, excluding the fat. These two flasks were kept for heating in a boiling water bath for half an hour and were allowed to cool down, slowing to ambient temperature. A few drops of phenolphthalein indicator were added to the flasks preceding the titration with KOH (0.5 N) until the pink color disappeared to white color. The endpoint was found to be 25.25 mL for the blank sample and 18.59 mL for the test sample. Saponification value is equal to mg of KOH consumed by 1 gm fat.

**Table 1.** Physiochemical properties of Kapok oil.

Oil extraction yield	23%
Acid value	18.541 mg KOH/g oil
Free fatty acid	9.317%
Saponification Value	186.813 mg KOH/g Fat
Specific gravity (at 20 °C)	0.850
pH	5.0
Kinematic viscosity (at 30 °C)	40 cSt

The saponification value was calculated using Equation (2).

$$\text{Saponification Value} = \frac{(B - T) \times 28.05}{\text{Weight of fat}} \quad (2)$$

where *B* = blank volume (mL) of KOH consumed per gram of fat, *T* = tested volume (mL) of KOH consumed per gram of fat [5].

### 2.6. Catalytic Transesterification Assisted by Ultrasonication

The biodiesel formation reaction in presence of catalyst was performed using an ultrasound bath. The bath consists of a turbine impeller with six blades, an immersed glassy reactor 45 mm in inner diameter with a capacity of 0.05 liters maintained at three inches height from its bottom surface, and a transducer (25 kHz). The ultrasonic bath is operated at its highest delivery value with 15% duty, switching on and off-cycle after 15 min. The reactor containing methanol and oil in a 6:1 ratio was stirred at 100 rpm for a reaction time of 4 h at an optimum temperature of 60 °C with 10% catalysts loading. The product of the reaction is FAME with glycerol as a byproduct of some unconverted methanol and catalysts. These are then moved into a rotary evaporator flask to recover unconverted methanol as well as the immobilized catalyst [8,14].

## 3. Results and Discussion

### 3.1. Textural Characterization

The crystalline nature of magnetite samples was investigated by the XRD technique as per procedure [35], presented in Figure 1a. The results showed that the sample has peaks at  $2\theta$  of 30.36°, 35.74°, 43.52°, 53.95°, 57.34° and 63.0°, indicating their spinel phase structures are in good agreement with the XRD standards for magnetite nanoparticles. The average size of particles was estimated by the Debye-Scherrer Equation, as in Equation (3) [35].

$$d = \frac{(k \times \lambda)}{(\beta \times \cos \theta)} \quad (3)$$

where  $d$  represents the particle size,  $\theta$  represents Bragg diffraction angle,  $k$  is Sherrer constant (0.9),  $\lambda$  is the wavelength of X-ray (0.15406 nm) and  $\beta$  represents the width of the XRD peak at half maxima. The average crystallite sizes of the magnetic Fe<sub>3</sub>O<sub>4</sub>-NPs are in the range of 17–25 nm. FTIR spectroscopy was used to identify the functional groups of the active components based on the peak value in the region of infrared radiation [36]. The iron oxide nanoparticles (Fe<sub>3</sub>O<sub>4</sub>-NPs) were prepared by the co-precipitation method and centrifuged for 2 min to isolate the Fe<sub>3</sub>O<sub>4</sub>-NPs from the compounds present in the solution. The FTIR spectrum of the as-synthesized magnetite (shown in Figure 1b) exhibited characteristic bands at 573 cm<sup>-1</sup> of magnetite, and the occurrence of a strong absorption peak at 590 cm<sup>-1</sup> is ascribed to the Fe-O bond of Fe<sub>3</sub>O<sub>4</sub> [35].

### 3.2. Temperature and Reaction Time Affecting the Yield of Biodiesel

Ultrasonic cavitation provides the necessary activation energy to increase the rate of reaction since ultrasonic cavitation enhances the mixing [37]. From Figure 2a, the conversion of biodiesel gradually increased from 53.2 ± 1.03% to 88.2 ± 0.58% with increased reaction time from 1 to 4 h at a constant temperature of 60 °C under a reactant molar ratio (methanol to Kapok oil) of 6:1, catalyst loading of 10 wt% and stirring at 100 rpm was observed, and the rate of conversion quickly reached 88.2 ± 0.58% during the first 4 h and the conversion of 88.54 ± 1.13% was detected after 4 h. The reason for the conversion rate being constant after 4 h is due to the buildup of the product on the active sites resulting in less availability of active surface area for the reaction and the reversible nature of the transesterification reaction. On the other hand, as depicted in Figure 2b, on increasing the temperature of the transesterification reaction from 40 °C to 70 °C, with other parameters remaining constant, the conversion was gradually increased from 28.1 ± 1.13% to 92.4 ± 0.91%, and the highest conversion of 92.4 ± 0.91% was observed at a reaction temperature of 70 °C and a 4 h reaction time. At a constant reaction temperature of 60 °C, for varying reaction times of 1 h, 2 h, 3 h and 4 h, respectively, the conversions were observed to be 51.2 ± 0.83%, 68.1 ± 0.99%, 75.4 ± 0.97%, and 88.6 ± 1.06%, and there are no more changes in the conversion of biodiesel after 4 h of the reaction time as the available surface area of the catalyst decreased and the process reached steady-state. The results can be explained as the lower viscosity of the reaction mixture at elevated temperatures increases cavitation,

leading to enhancement in the mass transfer rate and biodiesel production. In addition, there was a decrease in the activity of the catalyst at elevated temperatures due to the thermal denaturation of the catalyst. Therefore, taking into consideration both the aspect of temperature and reaction time, the optimum temperature was found to be 60 °C in this study with a conversion of  $88.6 \pm 1.06\%$  biodiesel. Similar work has been reported in Table 2.

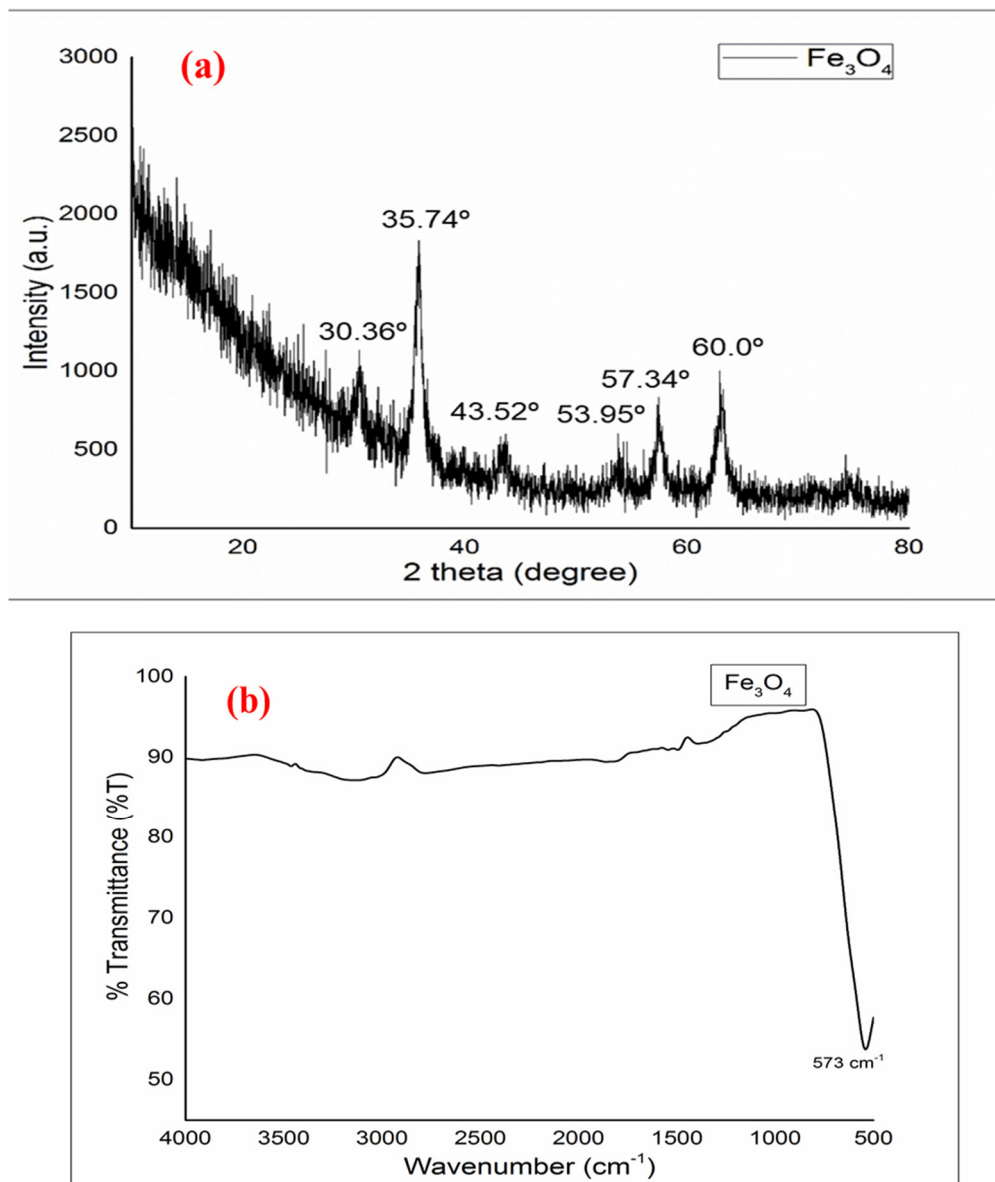


**Figure 1.** Haracterizations of magnetite (a) XRD pattern of the magnetite; (b) FTIR spectrum of the magnetite.

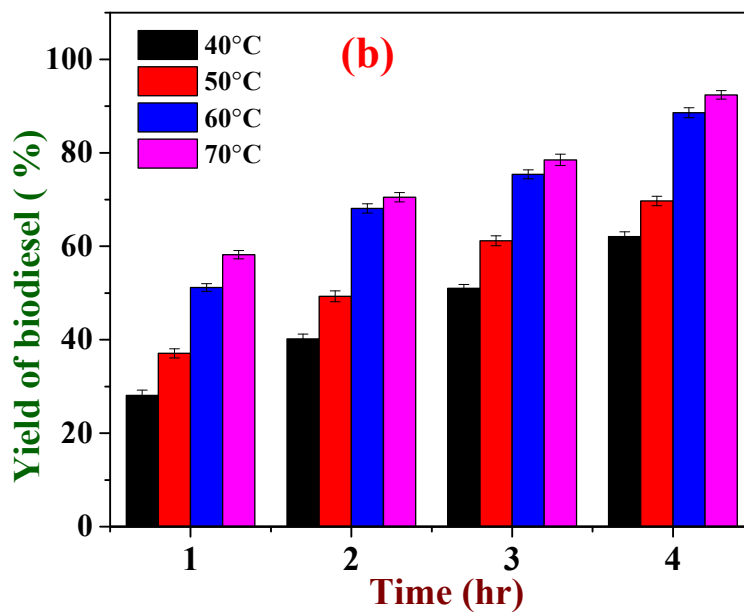
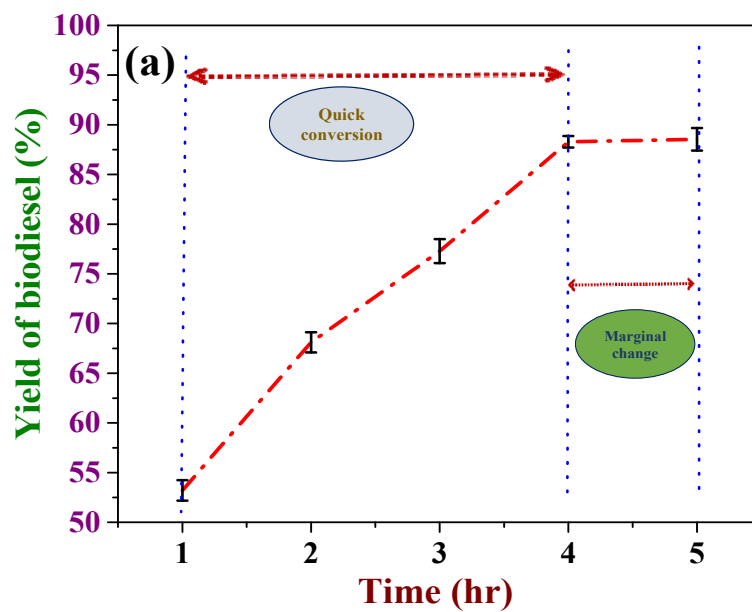


Figure 2. The yield of biodiesel (a) Effect of reaction time at temperature 60 °C; (b) Effect of temperature 40 °C to 70 °C, respectively.

Table 2. Production of biodiesel using ultrasound-assisted biocatalyst transesterification by different feedstocks.

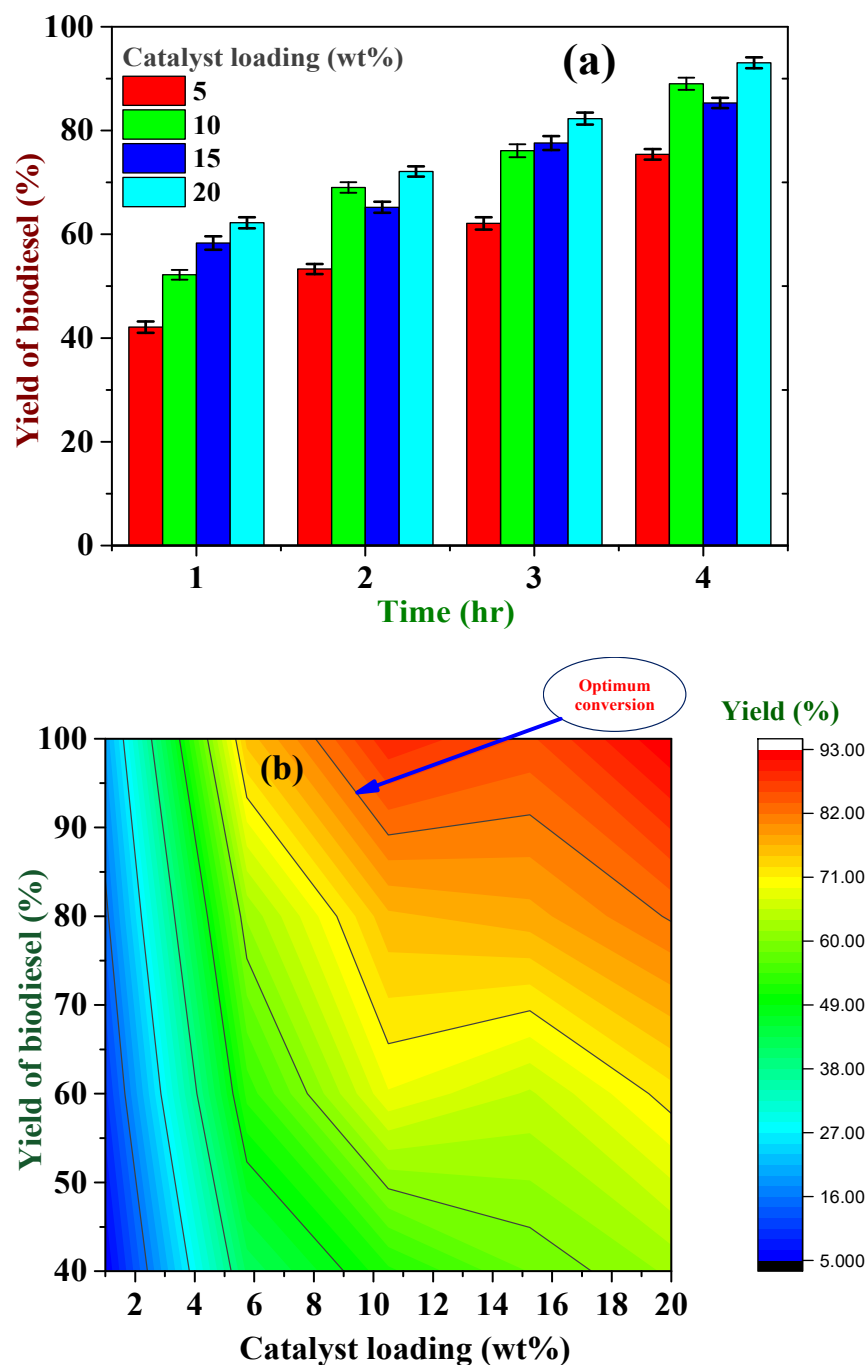
Feedstock	Bio-Catalyst	Alcohol/Oil	Reaction Condition	Yield	Ref.
Waste cottonseed oil	Immobilized Rhizopus oryzae lipase	Ethanol/oil molar ratio: 4.5:1	Temperature: 45 °C, Reaction time: 6 h Frequency: 20 kHz	98.7%	[38]
Waste cooking oil	Immobilized enzyme Novozym 435	Dimethyl carbonate/oil molar ratio: 6:1	Temperature: 70 °C, Reaction time: 4 h Frequency: 25 kHz	86.61%	[18]

Table 2. Cont.

Feedstock	Bio-Catalyst	Alcohol/Oil	Reaction Condition	Yield	Ref.
Waste tallow	Immobilized <i>Candida antarctica</i> lipase B (CALB)	Methanol/ fat molar ratio:8:1	Temperature: 50 °C, Reaction time: 20 min Frequency: 20 kHz	85.6 ± 0.08%	[39]
Canola oil	<i>T. lanuginosa</i> lipase immobilized on mesoporous silica/superparamagnetic iron oxide	Methanol/oil molar ratio:4.34	Reaction time: 6 h Frequency: 40 kHz	83.77%	[40]
<i>Jatropha curcas</i> oil	<i>Chromobacterium viscosum</i> lipase on immobilized silica activated	Methanol/oil molar ratio:4:1	Reaction time: 30 min Frequency: 30 kHz	84.5 ±0.5%	[41]
<i>Jatropha</i> oil	<i>E. aerogenes</i> and <i>Rhizopus oryzae</i> 3562 lipase immobilized on silica activated	Methanol/oil molar ratio:4:1	Temperature: 55 °C, Reaction time: 48 h	94%	[42]
Cooking oil	PDA-lipase immobilized on Fe <sub>3</sub> O <sub>4</sub> -	Methanol/oil molar ratio:6:1	Temperature: 37 °C, Reaction time: 30 h	92%	[43]
Kapok oil	<i>Rhizopus-oryzae</i> lipase immobilization on magnetic Fe <sub>3</sub> O <sub>4</sub> -NPs	Methanol/oil molar ratio:6:1	Temperature: 60 °C, Reaction time: 4 h Frequency: 25 kHz	93 ± 1.04%	<b>This work</b>

### 3.3. Effect of Catalysts Loading on the Yield of Biodiesel

Due to the high cost of enzymes, it is important to optimize the number of catalysts in the reaction. The amount of immobilized catalysts used for the reaction is a critical aspect in deciding the cost of production and the applicability at the industrial scale. To examine the effect of catalyst loading on the transesterification, the reaction was carried out under ultrasonic irradiation at different reaction times. The catalyst loading was taken at 5 wt% to 20% (*w/w*) with constant methanol to oil molar ratio (6:1). The obtained results are depicted in Figure 3a. When the loading was increased from 5 wt% to 20 wt%, there is an increase in the yield of biodiesel from 75.4 ± 1.02% to 93 ± 1.04% after 4 h. It is noteworthy that since the reaction involved enzymatic catalysis, where the catalyst and reactants are in a different phase, the application of ultrasonication in the transesterification reaction played a vital role in the conversion of biodiesel. In comparison to the conventional method, ultrasonic cavitation provides better mixing by reducing the required activation for the chemical reaction to occur thereby increasing the catalyst efficiency. Hence, the catalyst reactivity is enhanced with the increased availability of surface area to reactants. As a result of this, optimum conversion was achieved even at a lower catalyst loading of 10%, which is in good agreement with the previous result [41]. Increasing the catalyst loading to 20% did not necessarily result in an increment of conversion. On the contrary, a slight decrement from 89 ± 1.17% to 85.3 ± 0.98% was observed. Another possible explanation for such behavior is the aggregation of the catalyst. The kapok oil generally affected the interface of the catalyst while activation of the catalysts unmasked and restructured the active site through conformational changes of the enzyme's molecule. The increased catalyst loading increased the hydrolysis of the kapok oil, which in turn increased the water molecule on the interface, which aggregated the catalysts and blocked the available surface area of the catalyst to reduce the active sites [44]. The excess catalyst concentration has also increased the viscosity of mixing in the oil-water interface and reduced the limits of mass transfer [45,46], and therefore, the activity of the catalyst gradually decreased with an increase in the loading. Therefore, even after 15 wt% of catalyst, loading did not necessarily increase the conversion of biodiesel significantly. As illustrated in the isopleth in Figure 3b, the optimum yield region of biodiesel has been established, and the catalyst loading of 10 wt% was found to be an optimum concentration to minimize the hydrolysis of the methanol to oil and maximize the activity of the catalyst.



**Figure 3.** (a) Effect of catalyst loading on yield of biodiesel at optimum temperature of 60 °C for varying reaction time; (b) The optimum yield region isopleth diagram.

### 3.4. Characterizations of Kapok Biodiesel

The GC-MS analysis has been carried out for the kapok biodiesel as per the standard procedure [47]. The original kapok oil extracted demonstrated the presence of major fatty acids between C11:0 and C24:0 as undecylic acid, tridecylic acid, pentadecylic acid, ginkgolic acid, myristic acid, oleic acid, margaric acid, gondoic acid, arachidic acid, behenic acid, tricosanic acid and lignoceric acid [47,48]. Among the resulting fatty acids, short-chain hydrocarbons between C11:0 and C15:0 hold the major mass fraction composition, and transesterification leads to a reduction in the content of the FFA value.

The FAME in the Kapok biodiesel was identified through GC-MS in Figure 4 and tabulated in Table 3. The obtained values in GC-MS were compared with GC-MS library

data to determine the components in the unknown spectrum. Hydrocarbon grouping is differentiated as <C14, C14–C20 and C20–C30 to the retention time of standard hydrocarbons and molecular carbon chain length. The prepared KOMe (Kapok oil methyl ester) contains (C<sub>17</sub>H<sub>32</sub>O<sub>2</sub>) 20.44% of the peak area [49,50]. The average molecular weight of FAME in Kapok biodiesel is 288.387 (gm/gm mole) and was determined by Equation (4).

$$\text{The average molecular weight of Kapok biodiesel} = \sum_{i=1}^N (X_i \times M_i) \quad (4)$$

where  $X_i$  is the composition of hydrocarbon  $i$  and  $M_i$  is the molecular weight of Hydrocarbon  $i$ .

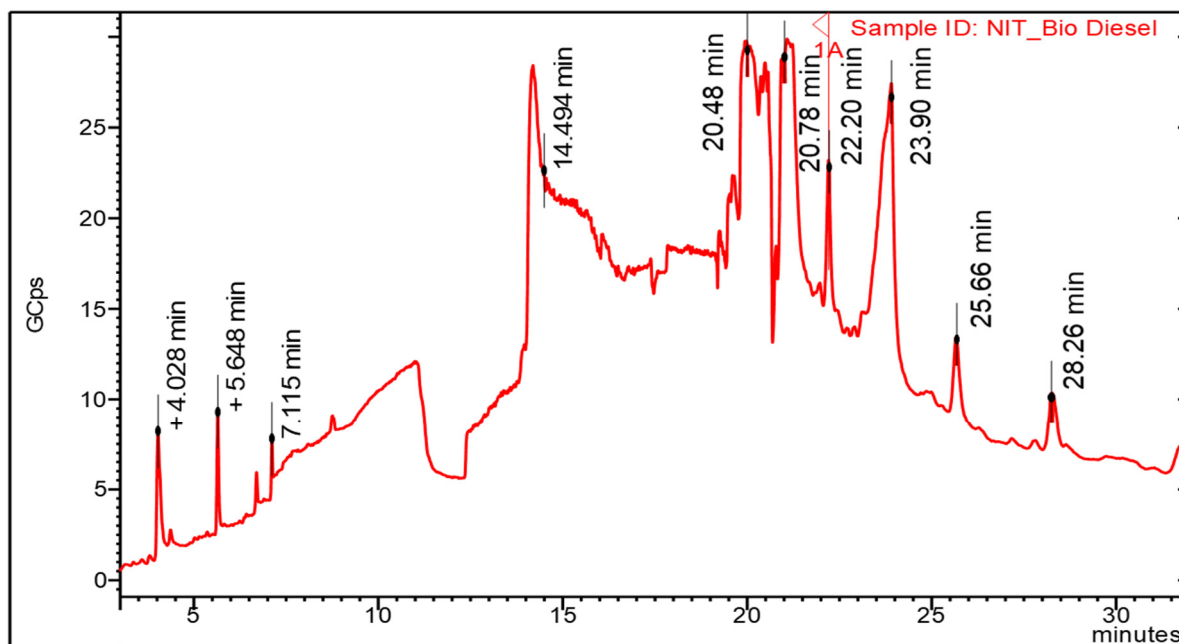


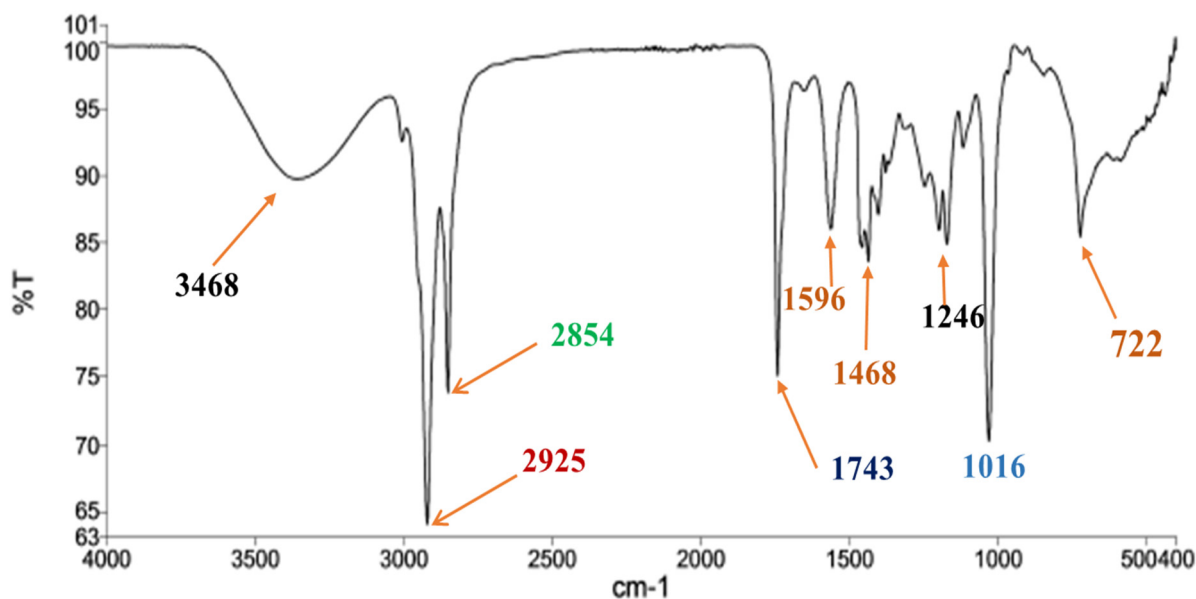
Figure 4. GC-MS Chromatogram of Kapok biodiesel.

Table 3. Major fatty acids of Kapok oil-derived Biodiesel as per GC-MS analysis.

Retention Time (min)	Component Name	Molecularweight	Composition (%)
4.028	13-Tetradecynoic acid, methyl ester	238	1.283
5.648	13,16-Octadecadiynoic acid, methyl ester	290	10.275
7.115	Nonanoic acid, methyl ester	172	2.209
14.494	Pentadecanoic acid, methyl ester	270	16.984
20.480	7-Hexadecenoic acid, methyl ester	268	20.439
20.78	Docosanoic acid, methyl ester	354	1.607
22.20	Tricosanoic acid, methyl ester	368	3.992
23.90	Tetracosanoic acid, methyl ester	382	15.862
25.66	Pentacosanoic acid, methyl ester	396	1.988
28.26	Hexacosanoic acid, methyl ester	410	1.501

Additionally, the presence of various functional groups of Kapok biodiesel was identified by FTIR spectrums following standard procedure [47] and depicted in Figure 5 to confirm the progress of biodiesel formation with the presence of volatile compounds at varying bending vibrations as alcohols, aldehydes, esters, alkanes, and derivatives of carboxylic acid. The occurrence of the weak-medium peak at 722 cm<sup>-1</sup> and 880 cm<sup>-1</sup> showed the presence of aromatic alkyne group -CH<sub>2</sub> and benzene derivatives (branched along with Cl and Br). Esters (RCOOR) are known to be phenomenal components for biodiesel, contributing to the major stretching areas between 1016 cm<sup>-1</sup> to 1246 cm<sup>-1</sup> and the signal at 1743 cm<sup>-1</sup> with continuous, broad, strong-medium signal. The peak in the

region of  $1743\text{ cm}^{-1}$  with C=O group and stretch vibration corresponds to the presence of the carbonyl group, and peaks at  $2925\text{ cm}^{-1}$  and  $2854\text{ cm}^{-1}$  correspond to the presence of an alkane group with C-H bonding and stretch vibration characteristics. The existence of carboxylic derivative (C-H) is identified by the inconsistent strong signal obtained at areas of  $2854\text{ cm}^{-1}$  and  $2925\text{ cm}^{-1}$ . The medium signals found at  $1363\text{ cm}^{-1}$  to  $1465\text{ cm}^{-1}$  and  $3468\text{ cm}^{-1}$  showed the presence of phenols, aldehydes, and alkene groups at a very minimal level. A peak at  $3468\text{ cm}^{-1}$  for the alcohol functional group was recorded with the O-H group and stretch vibration. Peaks in the region of  $1596\text{ cm}^{-1}$  and  $1465\text{ cm}^{-1}$  indicated fat and aromatic components with C=C group by stretch vibration [47].



**Figure 5.** FTIR spectrum of Kapok biodiesel.

Biodiesel of kapok oil was identified with  $^1\text{H-NMR}$  spectroscopy, which classifies the presence of hydroxyl functional groups at various places of a carbon chain [51].  $^1\text{H NMR}$  spectrum of Kapok oil biodiesel is presented in Figure 6. The presence of alkyl, alkynes, ethers, alcohols with  $\alpha$ -proton shift and esters are observed. The peak appearing between 1.32 ppm to 2.82 ppm confirmed the presence of alkyl and alkyne groups with the  $\alpha$ -proton shift. A peak with medium signals between 3.52 ppm to 3.67 ppm indicates the presence of ethers and alcohols. However, the occurrence of the peak between 3.84 to 4.18 ppm ensures the presence of the esters in major composition and 5.36 ppm ensures the presence of alkenes [48,52].

### 3.5. Kinetic and Thermodynamic Modeling of the Transesterification Process

The triglycerides of kapok oil are converted to methyl ester on the immobilized magnetite catalyst surface, and an excess amount of methanol is used to increase the miscibility of methanol and produce higher methyl esters. The methanol/oil molar ratio should be higher than that of the stoichiometric ratio to drive the reaction towards completion to produce the maximum methyl esters and prevent the backward reaction according to Le Chateleur's principle [27,53]. The chemical reactions of triglycerides were split into three steps: adsorption; surface reaction; and desorption. The surface reaction is considered as the rate-determining step of transesterification reaction, which involves the breaking and formation of bonds during the chemical reaction to generate methyl ester with the help of a catalyst during the reaction, and the three consecutive reversible reactions (5a) [12], adsorption reaction (5b), surface reaction (5c), desorption (5d) and overall reactions (5e) are illustrated in Table 4. Where  $[C_{OS}]$  and  $[S]$  are the overall surface concentration of the catalyst and vacant site of the catalyst,  $[C_{TG}]$ ,  $[C_{TG.S}]$ ,  $[C_{GL.S}]$  and  $[C_{MeOH}]$  are the concentration of triglycerides, adsorbed triglyceride at the active site, adsorbed glycerol on

the active site and concentration of methanol.  $K_{ads}$ ,  $K_{des}$  and  $K_s$  are the equilibrium rate constants of adsorption, desorption, and surface reaction.  $r_{ad}$ ,  $r_d$  and  $r_s$  are the rates of adsorption, desorption and surface reaction and  $r_{FAME}$  is the rate of overall triglycerides reaction. Here  $k_{ar}$  and  $k_{ap}$  are the forward and backward rate constants of the adsorption reaction between triglycerides and the catalyst.  $k_{sr}$  and  $k_{sp}$  are the forward and backward rate constants of the surface reaction with methanol.  $k_{dr}$  and  $k_{dp}$  are the forward and backward rate constants during desorption of the catalyst from glycerol.

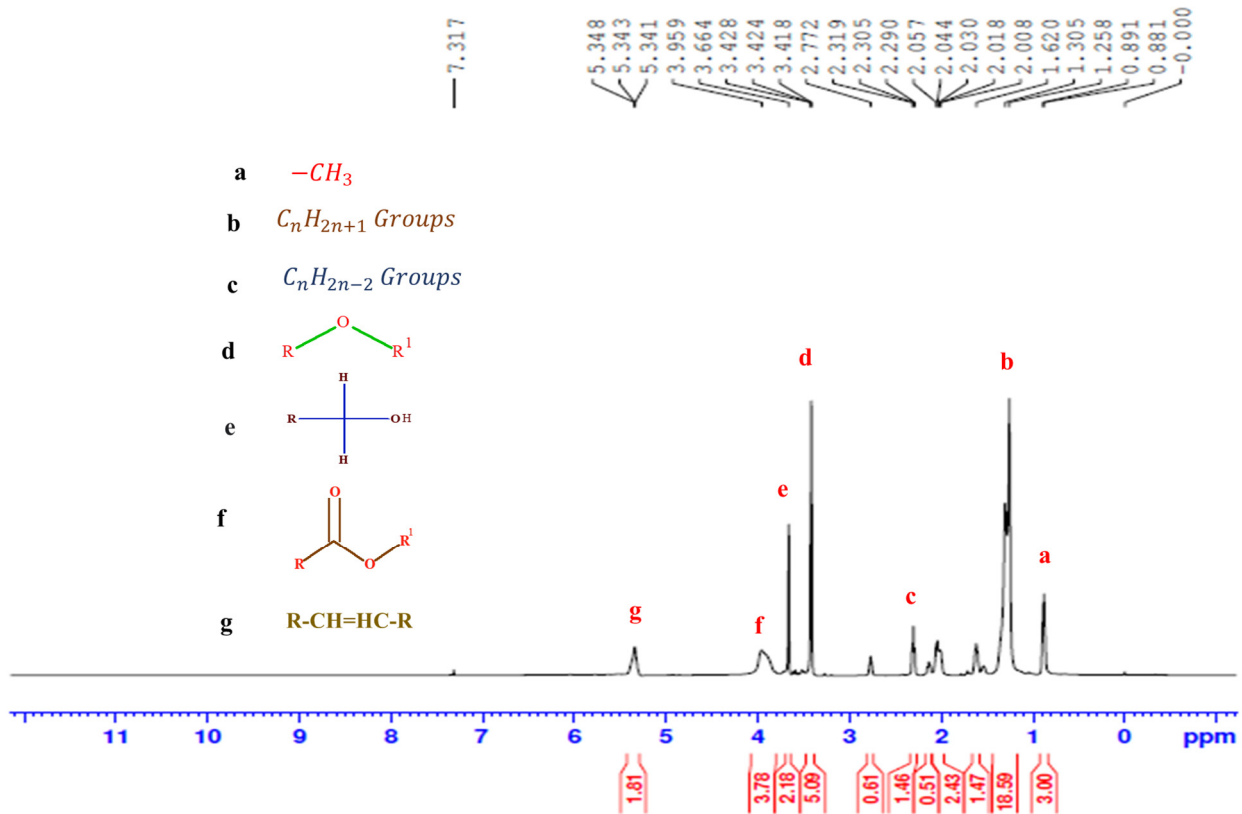


Figure 6. H-NMR spectrum of Kapok biodiesel to analyze the carbon chain.

Table 4. Catalytic transesterification reactions.

Consecutive Reversible Reactions of Triglyceride			Equation
			(5a)
Step Reactions	Rate Equations	Equilibrium Constants	
Adsorption reaction $TG \xrightleftharpoons[\text{magnetite-nanocatalyst}]{} TG.S$	$r_{ad} = k_{ar}[C_{TG}][S] - k_{ap}[C_{TG}.S]$	At $r_{ad} = 0$ , $K_{ads} = \frac{k_{ar}}{k_{ap}} = \frac{[C_{TG}.S]}{[C_{TG}][S]}$	(5b)
Surface reaction $TG.S + MeOH \leftrightarrow GL.S + FAME$	$r_s = k_{sr}[C_{TG}.S][C_{MeOH}] - k_{sp}[C_{GL}.S][C_{FAME}]$	At $r_s = 0$ , $K_s = \frac{k_{sr}}{k_{sp}} = \frac{[C_{GL}.S][C_{Biodiesel}]}{[C_{TG}.S][C_{MeOH}]}$	(5c)
Desorption reaction $GL.S \leftrightarrow GL + S$	$r_d = k_{dr}[C_{TG}.S] - k_{dp}[C_{GL}][S]$	At $r_d = 0$ , $K_{des} = \frac{k_{dr}}{k_{dp}} = \frac{[C_{GL}][S]}{[C_{TG}.S]}$	(5d)
Overall reaction $TG + 3MeOH \leftrightarrow GL + 3FAME$	$r_{FAME} = -\frac{dC_{TG}}{dt} = k[C_{TG}][C_{MeOH}]^3$	Rate constant at a constant amount of $MeOH$ $k_1 = k[C_{MeOH}]^3$	(5e)

The surface reaction was the slowest process. Thus the rate of adsorption (5a) and desorption (5d) can be neglected. Hence overall surface concentration is the sum of the vacant surface concentration, the concentration of adsorbed triglyceride, and the concentration of the adsorbed glycerol, as described in Equation (6). From Table 4, the equilibrium rate constants of adsorption, surface reaction, and desorption are rearranged and substituted in Equations (6) and surface rate Equation (5c) to obtain Equations (7) and (8) [5,10,54].

$$[C_{OS}] = [C_{GL.S}] + [S] + [C_{TG.S}] \tag{6}$$

$$[S] = \frac{[C_{OS}]}{(1 + K_{ads}[C_{TG}] + \frac{[C_{GL}]}{K_{des}})} \tag{7}$$

$$r_s = \frac{k_{sr} \cdot K_{ads} \cdot C_{OS} \cdot C_{MeOH} [C_{TG}] - \frac{C_{GL} C_{Biodiesel}}{K_s \cdot C_{MeOH}} [C_{TG}]}{(1 + K_{ads}[C_{TG}] + \frac{[C_{GL}]}{K_{des}})} = k_1 \cdot C_{TG} \tag{8}$$

In the catalytic transesterification reaction, the rate of adsorption is much less and the rate of desorption is very high on the catalyst. However both terms  $K_{ads}[C_{TG}]$  and  $\frac{[C_{GL}]}{K_{des}}$  are considered as zero, and glycerol is immiscible into the mixture of biodiesel-MeOH due to low solubility ( $[C_{GL}] = 0$ ), so the surface reaction is purportedly not favorable to the reversible side. Therefore during the transesterification reaction, the excess amount of methanol was used ( $[C_{MeOH}] \gg [C_{TG}]$ ), meaning change in concentration of methanol is negligible, and thus all final rate constants can be set as  $k_1$  in Equation (8), whereas  $k_1$  implies the final rate constant and is equal to the  $k_{sr} \cdot K_{ads} \cdot C_{OS} \cdot C_{MeOH}$ , indicating a pseudo-first-order kinetic for the surface reaction and overall reaction. The overall transesterification reaction (5e) is listed according to Equation (5a), where three moles of MeOH are required and  $k$  is the rate constant. From the above surface reaction discussion, a pseudo-first-order kinetic model for the transesterification reaction was assumed in Equation (9) since the amount of methanol is fixed. From the rate of surface reaction in Equation (8) to the overall transesterification reaction in Equation (9), the rate of both reactions are mathematically and theoretically proved as pseudo-first-order kinetic models.

$$r_{FAME} = -\frac{dC_{TG}}{dt} = k_1[C_{TG}] = -\int_{dC_{TG}0}^{dC_{TG}} \frac{dC_{TG}}{C_{TG}} = k_1 \int_0^t dt \tag{9}$$

Equation (9) can be integrated with boundary condition time at 0 to t to obtain Equation (10).

$$\ln \frac{1}{(1 - X_{FAME})} = k_1 t \tag{10}$$

where  $k_1 = k[C_{MeOH}]^3$  is the rate constant ( $h^{-1}$ ) based on the mass balance obtained in Equation (9) and  $r_{FAME}$  is the rate of reaction of triglycerides,  $C_{TG}$  is the final concentration of triglycerides at time t,  $C_{TG0}$  is the initial concentration of triglycerides at time 0,  $X_{FAME}$  represents the conversion of triglyceride at a given time t.

Values of rate constants calculated using Equation (10) for given reaction time and temperatures from 40 °C to 70 °C by the corresponding regression equations are shown in Table 5. These temperatures were under the range of liquid and vapor phases of MeOH in the reaction. When the reaction was conducted above the boiling point of methanol (65 °C), bubbles were formed in the solution, which increased the evaporation rate. This rate of evaporation affected the mass transfer on the interface and decreased the mixing

time between methanol and oil, causing a decrease in the formation of biodiesel above the boiling point of methanol. However, in Figure 2b, the yield of the biodiesel increased even at 70 °C as a result of ultrasonication. The ultrasonication provided the energy to generate the cavitation bubbles and micro-emulsion by mixing methanol/oil to support the maximum temperature (70 °C) near the interface of the immiscible phase [19].

**Table 5.** Effect of the temperature vs. time.

Temperature (°C)	Regression Equation	R <sup>2</sup>	Rate Constant $k_1$ (h <sup>-1</sup> )
40	$y = 0.2124x + 0.1006$	0.994	0.212
50	$y = 0.2459x + 0.2062$	0.998	0.246
60	$y = 0.4622x + 0.2029$	0.953	0.466
70	$y = 0.5423x + 0.1965$	0.908	0.542

The relation between rate constant and temperature is stated by the Arrhenius Equation (11) [5].

$$\ln k_1 = \left( -\frac{E_a}{R} \right) \frac{1}{T} + \ln k_0 \quad (11)$$

where,  $R$ ,  $k_1$ ,  $k_0$  and  $E_a$  are denote the gas constant (8.314 J mol<sup>-1</sup> K<sup>-1</sup>), rate constant (h<sup>-1</sup>), the pre-exponential factor (h<sup>-1</sup>), and activation energy (kJ mol<sup>-1</sup>), respectively. From Equation (11), a linear correlation exists between  $\ln k_1$  and  $1/T$ . Therefore, the Arrhenius parameters  $k_0$  and  $E_a$  are evaluated by regression linear methods,  $\frac{E_a}{R}$  represents the slope and  $\ln k_0$  is the intercept. An equation  $\ln k_1$  vs  $1/T$  gives a linear regression to prove the pseudo-first-order kinetic was well fit to the transesterification process. The values of  $k_0$  and  $E_a$  of the transesterification reaction were determined as 27,446.66 h<sup>-1</sup> and 30.79 kJ mol<sup>-1</sup>. A higher value of rate constant and lower value of activation energy specifies that the rate of transesterification reaction was fast using an immobilized catalyst. Very few studies have been dedicated to understanding the kinetics of the transesterification process via ultrasonic systems with catalysts. The activation energy reported was 33.6–84 kJ mol<sup>-1</sup> [18,27,55]. In comparison, the activation energy for the reaction in the present study is lower than the rest as a result of higher mass transfer rates and higher yield of the biodiesel.

Furthermore, the thermodynamic properties of the transesterification reaction were determined by the “Eyring-Polanyi” theory, and the reaction rate can be expressed as Equation (12).

$$\ln\left(\frac{k_1}{T}\right) = \left(-\frac{\Delta H}{R}\right) \frac{1}{T} + \left\{ \ln\left(\frac{k_b}{h}\right) + \frac{\Delta S}{R} \right\} \quad (12)$$

Then Gibbs’s free energy can be calculated by Equation (13) [55].

$$\Delta G = (-\Delta S)T + \Delta H \quad (13)$$

where  $k_1$  is the rate constant (s<sup>-1</sup>), at temperature  $T$  (K),  $k_b$  = Boltzmann constant (1.38 × 10<sup>23</sup> J/K),  $h$  = Planck’s constant (6.63 × 10<sup>-34</sup> J. s),  $\Delta H$  = enthalpy of activation (kJ mol<sup>-1</sup>),  $\Delta S$  = entropy of activation (J mol<sup>-1</sup> K<sup>-1</sup>),  $\Delta G$  = Gibbs free energy (kJ mol<sup>-1</sup>). The value of the standard enthalpy ( $\Delta H$ ) and entropy ( $\Delta S$ ) for the transesterification reaction was determined from the slope and intercept of the Eyring plot ( $\ln(\frac{k_1}{T})$  vs.  $\frac{1}{T}$ ) as shown in Figure 7a. The values of the thermodynamic properties of the transesterification reaction are given in Table 6, indicating the positive value of  $\Delta H$  heat input is required to raise the energy level for the reactant to transform to their transition state from the product [56]. The reaction temperature has a strong influence on the rate of biodiesel production as the reaction was typically endothermic. The negative value of entropy ( $\Delta S$ ) indicates that the degree of ordered alignment of the transition state is better as compared to reactant in the ground state. In Figure 7b, the positive value of Gibbs free energy ( $\Delta G$ ) indicates that the reaction was unspontaneous and endergonic [57]. The immobilized magnetite catalyst-based

transesterification reaction of Gibbs free energy and enthalpy are comparatively better than those of the heterogeneous and homogenous catalytic transesterification reaction and only a few works have been reported in the literature [24,27,55].

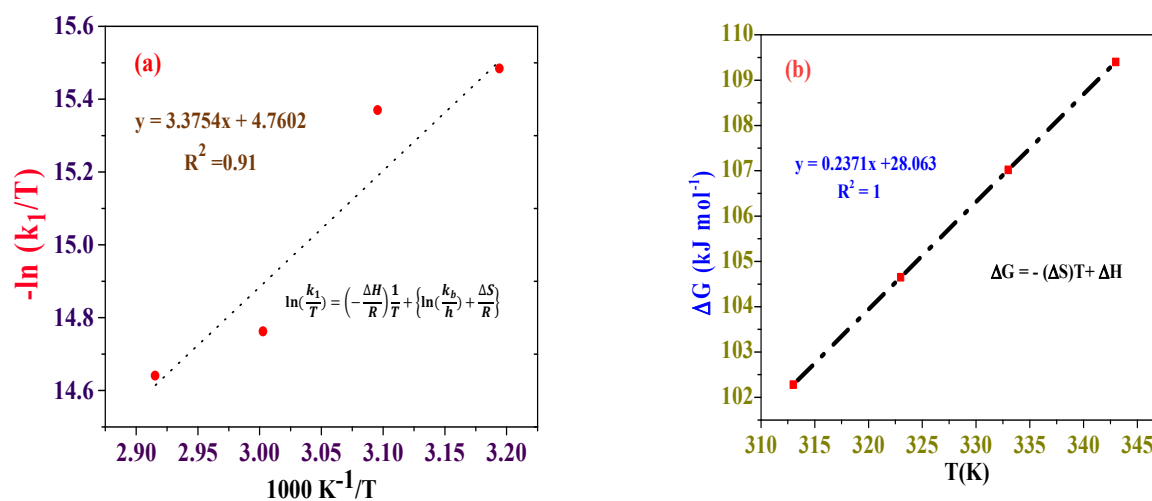


**Figure 7.** (a) The Eyring plot ( $1/T$  vs  $\ln k/T$ ); (b) A plot of  $\Delta G$  vs.  $T$  of used catalyst-based transesterification reaction.

**Table 6.** Different thermodynamic parameters with calculated values of the transesterification reaction.

Terms	Description	Value
$k_0$	Frequency factor ( $h^{-1}$ )	27,446.66
$\Delta E$	Activation Energy ( $kJ mol^{-1}$ )	30.79
$\Delta H$	Enthalpy ( $kJ mol^{-1}$ )	28.06
$\Delta S$	Entropy ( $J mol^{-1} K^{-1}$ )	-237.12
$\Delta G$	Gibbs free energy	( $kJ mol^{-1}$ )
	313 K	102.28
	323 K	104.65
	333 K	107.02
	343 K	109.40

#### 4. Conclusions

In summary, a simple and economical pathway for deriving biodiesel from Kapok (*Ceiba pentandra*) oil has been successfully developed with a thorough investigation into its thermodynamics as well as kinetics. An innovative technique is adopted using magnetic nanoparticles embedded in immobilized *Rhizopus oryzae* assisted by ultrasonication to initiate the transesterification reaction. Employing the co-precipitation method in an aqueous solution using single iron (III) salt the magnetite nanoparticles were synthesized. The produced biodiesel has no side products. The use of ultrasonication aided in lowering the activation energy of the pseudo first-order kinetic reaction to the lowest value ever reported achieving a conversion of  $93 \pm 1.04\%$  with minimum catalyst loading of 10 wt% within a short reaction time of 4 h and temperature of 60 °C. Besides, the employment of iron nanoparticles resulted in higher loading of the immobilized catalyst with the quick substrate-enzyme complex formation, which also contributed to the higher conversion. Thus the amalgamation of the bio-nanocatalyst together with ultrasonication demonstrated manifold advantages for generating a high yield of biodiesel employing an abundant non-agro based oilseed. The simplicity of the process makes it desirable over conventional routes to produce biodiesel with huge potential for scale-up from lab to industrial scale in the future.

**Author Contributions:** M.P.: Conceptualization, Methodology, Writing—original draft. B.D.: Validation, Formal analysis. H.-M.C.: Writing—review and editing. C.-T.C.: Writing—review. T.X.Q.N.: Project administration. S.-S.C.: Conceptualization, Supervision, Investigation, Writing—review and editing. H.-M.K. and Y.-F.C.: Funding acquisition, Resources, Writing—review and editing. All authors have read and agreed to the published version of the manuscript.

**Funding:** The authors would like to acknowledge, for this research are thankful to the financial supply from the Ministry of Science and Technology (MOST), Republic of China (Taiwan) under grant number 107-2221-E-027-001-MY3.

**Institutional Review Board Statement:** Not applicable.

**Informed Consent Statement:** Not applicable.

**Data Availability Statement:** The data presented in this study are available in the article.

**Conflicts of Interest:** The authors declare no conflict of interest.

## References

1. Loo, D.L.; Teoh, Y.H.; How, H.G.; Teh, J.S.; Andrei, L.C.; Starčević, S.; Sher, F. Applications Characteristics of Different Biodiesel Blends in Modern Vehicles Engines: A Review. *Sustainability* **2021**, *13*, 9677. [\[CrossRef\]](#)
2. Gui, M.M.; Lee, K.; Bhatia, S. Feasibility of Edible Oil vs. Non-Edible Oil vs. Waste Edible Oil as Biodiesel Feedstock. *Energy* **2008**, *33*, 1646–1653. [\[CrossRef\]](#)
3. Atabani, A.; Silitonga, A.; Badruddin, I.A.; Mahlia, T.M.I.; Masjuki, H.; Mekhilef, S. A Comprehensive Review on Biodiesel as an Alternative Energy Resource and its Characteristics. *Renew. Sustain. Energy Rev.* **2012**, *16*, 2070–2093. [\[CrossRef\]](#)
4. Shahid, E.M.; Jamal, Y. Production of Biodiesel: A Technical Review. *Renew. Sustain. Energy Rev.* **2011**, *15*, 4732–4745. [\[CrossRef\]](#)
5. Sivakumar, P.; Sindhanaiselvan, S.; Gandhi, N.N.; Devi, S.S.; Renganathan, S. Optimization and Kinetic Studies on Biodiesel Production from Underutilized Ceiba Pentandra Oil. *Fuel* **2013**, *103*, 693–698. [\[CrossRef\]](#)
6. Jamaluddin, N.; Riayatsyah, T.M.I.; Silitonga, A.S.; Mofijur, M.; Shamsuddin, A.H.; Ong, H.C.; Mahlia, T.M.I.; Rahman, S.A. Techno-Economic Analysis and Physicochemical Properties of Ceiba Pentandra as Second-Generation Biodiesel Based on ASTM D6751 and EN 14214. *Processes* **2019**, *7*, 636. [\[CrossRef\]](#)
7. Teoh, Y.; How, H.; Sher, F.; Le, T.; Nguyen, H.; Yaqoob, H. Fuel Injection Responses and Particulate Emissions of a CRDI Engine Fueled with *Cocos Nucifera* Biodiesel. *Sustainability* **2021**, *13*, 4930. [\[CrossRef\]](#)
8. Vedharaj, S.; Vallinayagam, R.; Yang, W.; Chou, S.; Chua, K.J.; Lee, P. Experimental Investigation of Kapok (*Ceiba pentandra*) Oil Biodiesel as an Alternate Fuel for Diesel Engine. *Energy Convers. Manag.* **2013**, *75*, 773–779. [\[CrossRef\]](#)
9. Cui, F.-J.; Zhao, H.-X.; Sun, W.-J.; Wei, Z.; Yu, S.-L.; Zhou, Q.; Dong, Y. Ultrasound-Assisted Lipase-Catalyzed Synthesis of D-isoascorbyl Palmitate: Process Optimization and Kinetic Evaluation. *Chem. Cent. J.* **2013**, *7*, 180. [\[CrossRef\]](#)
10. Sharma, A.; Kodgire, P.; Kachhwaha, S.S. Investigation of Ultrasound-Assisted KOH and CaO Catalyzed Transesterification for Biodiesel Production from Waste Cotton-Seed Cooking Oil: Process Optimization and Conversion Rate Evaluation. *J. Clean. Prod.* **2020**, *259*, 120982. [\[CrossRef\]](#)
11. Veljković, V.B.; Avramović, J.M.; Stamenković, O. Biodiesel Production by Ultrasound-Assisted Transesterification: State of the Art and the Perspectives. *Renew. Sustain. Energy Rev.* **2011**, *16*, 1193–1209. [\[CrossRef\]](#)
12. Zabeti, M.; Daud, W.M.A.W.; Aroua, M.K. Activity of Solid Catalysts for Biodiesel Production: A Review. *Fuel Process. Technol.* **2009**, *90*, 770–777. [\[CrossRef\]](#)
13. Borugadda, V.B.; Goud, V.V. Biodiesel Production from Renewable Feedstocks: Status and Opportunities. *Renew. Sustain. Energy Rev.* **2012**, *16*, 4763–4784. [\[CrossRef\]](#)
14. Batistella, L.; Lerin, L.A.; Brugnerotto, P.; Danielli, A.J.; Trentin, C.M.; Popiolski, A.; Treichel, H.; Oliveira, J.V.; de Oliveira, D. Ultrasound-Assisted Lipase-Catalyzed Transesterification of Soybean Oil in Organic Solvent System. *Ultrason. Sonochem.* **2012**, *19*, 452–458. [\[CrossRef\]](#)
15. Aguieiras, E.C.G.; Ribeiro, D.S.; Coutinho, P.P.; Bastos, C.M.B.; de Queiroz, D.S.; Parreira, J.M.; Langone, M.A.P. Investigation of the Reuse of Immobilized Lipases in Biodiesel Synthesis: Influence of Different Solvents in Lipase Activity. *Appl. Biochem. Biotechnol.* **2016**, *179*, 485–496. [\[CrossRef\]](#)
16. Amini, Z.; Ong, H.C.; Harrison, M.; Kusumo, F.; Mazaheri, H.; Ilham, Z. Biodiesel Production by Lipase-Catalyzed Transesterification of *Ocimum basilicum* L. (Sweet Basil) Seed Oil. *Energy Convers. Manag.* **2017**, *132*, 82–90. [\[CrossRef\]](#)
17. Vyas, A.P.; Verma, J.L.; Subrahmanyam, N. A Review on FAME Production Processes. *Fuel* **2010**, *89*, 1–9. [\[CrossRef\]](#)
18. Gharat, N.; Rathod, V.K. Ultrasound Assisted Enzyme Catalyzed Transesterification of Waste Cooking Oil with Dimethyl Carbonate. *Ultrason. Sonochem.* **2012**, *20*, 900–905. [\[CrossRef\]](#)
19. Santin, C.M.; Michelin, S.; Scherer, R.P.; Valério, A.; di Luccio, M.; Oliveira, D.; Oliveira, J.V. Comparison of Macauba and Soybean Oils as Substrates for the Enzymatic Biodiesel Production in Ultrasound-Assisted System. *Ultrason. Sonochem.* **2017**, *35*, 525–528. [\[CrossRef\]](#)

20. Kumar, D.; Kumar, G.; Poonam; Singh, C. Ultrasonic-Assisted Transesterification of Jatropha Curcus Oil Using Solid Catalyst, Na/SiO<sub>2</sub>. *Ultrason. Sonochem.* **2010**, *17*, 839–844. [[CrossRef](#)]
21. Ansari, S.A.; Husain, Q. Potential Applications of Enzymes Immobilized on/in Nano Materials: A Review. *Biotechnol. Adv.* **2012**, *30*, 512–523. [[CrossRef](#)]
22. Lerin, L.A.; Loss, R.A.; Remonato, D.; Zenevycz, M.C.; Balen, M.; Netto, V.O.; Ninow, J.L.; Trentin, C.M.; Oliveira, J.V.; De Oliveira, D. A Review on Lipase-Catalyzed Reactions in Ultrasound-Assisted Systems. *Bioprocess Biosyst. Eng.* **2014**, *37*, 2381–2394. [[CrossRef](#)] [[PubMed](#)]
23. Jegannathan, K.R.; Abang, S.; Poncelet, D.; Chan, E.S.; Ravindra, P. Production of Biodiesel Using Immobilized Lipase—A Critical Review. *Crit. Rev. Biotechnol.* **2008**, *28*, 253–264. [[CrossRef](#)] [[PubMed](#)]
24. Kim, K.H.; Lee, O.K.; Lee, E.Y. Nano-Immobilized Biocatalysts for Biodiesel Production from Renewable and Sustainable Resources. *Catalysts* **2018**, *8*, 68. [[CrossRef](#)]
25. Al-Zuhair, S.; Ling, F.W.; Jun, L.S. Proposed Kinetic Mechanism of the Production of Biodiesel from Palm Oil Using Lipase. *Process Biochem.* **2007**, *42*, 951–960. [[CrossRef](#)]
26. Moreira, K.D.S.; De Oliveira, A.L.B.; Lourembergue, S.d.M., Jr.; Monteiro, R.R.C.; Da Rocha, T.N.; Menezes, F.L.; Fechine, L.M.U.D.; Denardin, J.C.; Michea, S.; Freire, R.M.; et al. Lipase from *Rhizomucor Miehei* Immobilized on Magnetic Nanoparticles: Performance in Fatty Acid Ethyl Ester (FAEE) Optimized Production by the Taguchi Method. *Front. Bioeng. Biotechnol.* **2020**, *8*, 693. [[CrossRef](#)]
27. Santos, S.; Puna, J.; Gomes, J.; Marchetti, J. A Review on the Use of Bio/Nanostructured Heterogeneous Catalysts in Biodiesel Production. *Nano-Biocatal. Biodiesel Prod.* **2021**, 59–91. [[CrossRef](#)]
28. Gupta, A.K.; Gupta, M. Synthesis and Surface Engineering of Iron Oxide Nanoparticles for Biomedical Applications. *Biomaterials* **2005**, *26*, 3995–4021. [[CrossRef](#)]
29. Xie, W.; Ma, N. Immobilized Lipase on Fe<sub>3</sub>O<sub>4</sub> Nanoparticles as Biocatalyst for Biodiesel Production. *Energy Fuels* **2009**, *23*, 1347–1353. [[CrossRef](#)]
30. Xie, W.; Huang, M. Immobilization of *Candida Rugosa* Lipase onto Graphene Oxide Fe<sub>3</sub>O<sub>4</sub> Nanocomposite: Characterization and Application for Biodiesel Production. *Energy Convers. Manag.* **2018**, *159*, 42–53. [[CrossRef](#)]
31. Sun, J.; Zhou, S.; Hou, P.; Yang, Y.; Weng, J.; Li, X.; Li, M. Synthesis and Characterization of Biocompatible Fe<sub>3</sub>O<sub>4</sub> Nanoparticles. *J. Biomed. Mater. Res. Part A* **2007**, *80*, 333–341. [[CrossRef](#)] [[PubMed](#)]
32. Ashkevarian, S.; Badraghi, J.; Mamashli, F.; Delavari, B.; Saboury, A.A. Covalent Immobilization and Characterization of *Rhizopus Oryzae* Lipase on Core-Shell Cobalt Ferrite Nanoparticles for Biodiesel Production. *Chin. J. Chem. Eng.* **2020**, *37*, 128–136. [[CrossRef](#)]
33. Zhao, J.-F.; Lin, J.-P.; Yang, L.-R.; Wu, M.-B. Enhanced Performance of *Rhizopus oryzae* Lipase by Reasonable Immobilization on Magnetic Nanoparticles and Its Application in Synthesis 1,3-Diacylglycerol. *Appl. Biochem. Biotechnol.* **2019**, *188*, 677–689. [[CrossRef](#)] [[PubMed](#)]
34. Azad, A.; Rasul, M.; Khan, M.; Sharma, S.C.; Mofijur, M.; Bhuiya, M. Prospects, Feedstocks and Challenges of Biodiesel Production from Beauty Leaf Oil and Castor Oil: A Nonedible Oil Sources in Australia. *Renew. Sustain. Energy Rev.* **2016**, *61*, 302–318. [[CrossRef](#)]
35. Khalil, M.I. Co-Precipitation in Aqueous Solution Synthesis of Magnetite Nanoparticles Using Iron (III) Salts as Precursors. *Arab. J. Chem.* **2015**, *8*, 279–284. [[CrossRef](#)]
36. Azhar, O.; Jahan, Z.; Sher, F.; Niazi, M.B.K.; Kakar, S.J.; Shahid, M. Cellulose Acetate-Polyvinyl Alcohol Blend Hemodialysis Membranes Integrated with Dialysis Performance and High Biocompatibility. *Mater. Sci. Eng. C* **2021**, *126*, 112127. [[CrossRef](#)]
37. Gholami, A.; Pourfayaz, F.; Maleki, A. Techno-Economic Assessment of Biodiesel Production from Canola Oil through Ultrasonic Cavitation. *Energy Rep.* **2020**, *7*, 266–277. [[CrossRef](#)]
38. Yasvanthrajan, N.; Sivakumar, P.; Muthukumar, K.; Murugesan, T.; Arunagiri, A. Production of Biodiesel from Waste Bio-Oil through Ultrasound Assisted Transesterification Using Immobilized Lipase. *Environ. Technol. Innov.* **2020**, *21*, 101199. [[CrossRef](#)]
39. Adewale, P.; Dumont, M.-J.; Ngadi, M. Enzyme-Catalyzed Synthesis and Kinetics of Ultrasonic-Assisted Biodiesel Production from Waste Tallow. *Ultrason. Sonochem.* **2015**, *27*, 1–9. [[CrossRef](#)]
40. Karimi, M.; Keyhani, A.; Akram, A.; Rahman, M.; Jenkins, B.; Stroeve, P. Hybrid Response Surface Methodology-Genetic Algorithm Optimization of Ultrasound-Assisted Transesterification of Waste Oil Catalysed by Immobilized Lipase on Mesoporous Silica/Iron Oxide Magnetic Core-Shell Nanoparticles. *Environ. Technol.* **2013**, *34*, 2201–2211. [[CrossRef](#)]
41. Kumar, G.; Kumar, D.; Johari, R.; Singh, C.P. Enzymatic Transesterification of Jatropha Curcas Oil Assisted by Ultrasonication. *Ultrason. Sonochem.* **2011**, *18*, 923–927. [[CrossRef](#)] [[PubMed](#)]
42. Kumari, A.; Mahapatra, P.; Garlapati, V.K.; Banerjee, R. Enzymatic Transesterification of Jatropha Oil. *Biotechnol. Biofuels* **2009**, *2*, 1. [[CrossRef](#)] [[PubMed](#)]
43. Touqeer, T.; Mumtaz, M.W.; Mukhtar, H.; Irfan, A.; Akram, S.; Shabbir, A.; Rashid, U.; Nehdi, I.A.; Choong, T.S.Y. Fe<sub>3</sub>O<sub>4</sub>-PDA-Lipase as Surface Functionalized Nano Biocatalyst for the Production of Biodiesel Using Waste Cooking Oil as Feedstock: Characterization and Process Optimization. *Energies* **2019**, *13*, 177. [[CrossRef](#)]
44. Wang, X.; Qin, X.; Li, D.; Yang, B.; Wang, Y. One-Step Synthesis of High-Yield Biodiesel from Waste Cooking Oils by a Novel and Highly Methanol-Tolerant Immobilized Lipase. *Bioresour. Technol.* **2017**, *235*, 18–24. [[CrossRef](#)] [[PubMed](#)]

45. Subhedar, P.B.; Gogate, P.R. Ultrasound Assisted Intensification of Biodiesel Production Using Enzymatic Interesterification. *Ultrason. Sonochem.* **2016**, *29*, 67–75. [[CrossRef](#)]
46. Suslick, K. Applications of Ultrasound to Materials Chemistry. *MRS Bull.* **1995**, *20*, 29–34. [[CrossRef](#)]
47. Karthickeyan, V. Effect of Thermal Barrier Coating on Performance and Emission Characteristics of Kapok Oil Methyl Ester in Diesel Engine. *Aust. J. Mech. Eng.* **2018**, *18*, 467–480. [[CrossRef](#)]
48. Silva, L.M.; Filho, E.A.; Simpson, A.J.; Monteiro, M.R.; Venâncio, T. Comprehensive Multiphase NMR Spectroscopy: A New Analytical Method to Study the Effect of Biodiesel Blends on the Structure of Commercial Rubbers. *Fuel* **2015**, *166*, 436–445. [[CrossRef](#)]
49. Norjannah, B.; Ong, H.C.; Masjuki, H. Effects of Methanol and Enzyme Pretreatment to Ceiba Pentandra Biodiesel Production. *Energy Sources Part A Recover. Util. Environ. Eff.* **2017**, *39*, 1548–1555. [[CrossRef](#)]
50. Asokan, M.A.; Vijayan, R. Effective Conversion of Kapok Seed (Ceiba Pentandra) Oil into Biodiesel and Investigation of Effects of Catalyst Concentrations and Chromatographic Characterization. *Int. J. Chem. Tech. Res.* **2014**, *6*, 5709–5715.
51. Rashid, U.; Knothe, G.; Yunus, R.; Evangelista, R.L. Kapok Oil Methyl Esters. *Biomass-Bioenergy* **2014**, *66*, 419–425. [[CrossRef](#)]
52. Zhao, L.; Huang, Y.; Hu, J.; Zhou, H.; Adeleye, A.S.; Keller, A.A. <sup>1</sup>H NMR and GC-MS Based Metabolomics Reveal Defense and Detoxification Mechanism of Cucumber Plant under Nano-Cu Stress. *Environ. Sci. Technol.* **2016**, *50*, 2000–2010. [[CrossRef](#)] [[PubMed](#)]
53. Bajaj, A.; Lohan, P.; Jha, P.N.; Mehrotra, R. Biodiesel Production through Lipase Catalyzed Transesterification: An Overview. *J. Mol. Catal. B Enzym.* **2010**, *62*, 9–14. [[CrossRef](#)]
54. Endalew, A.K.; Kiros, Y.; Zanzi, R. Inorganic Heterogeneous Catalysts for Biodiesel Production from Vegetable Oils. *Biomass-Bioenergy* **2011**, *35*, 3787–3809. [[CrossRef](#)]
55. Feyzi, M.; Shahbazi, Z. Preparation, Kinetic and Thermodynamic Studies of Al–Sr Nanocatalysts for Biodiesel Production. *J. Taiwan Inst. Chem. Eng.* **2017**, *71*, 145–155. [[CrossRef](#)]
56. Teixeira, R.A.; Lima, E.C.; Benetti, A.D.; Thue, P.S.; Cunha, M.R.; Cimirro, N.F.; Sher, F.; Dehghani, M.H.; dos Reis, G.S.; Dotto, G.L. Preparation of Hybrids of Wood Sawdust with 3-Aminopropyl-Triethoxysilane. Application as an Adsorbent to Remove Reactive Blue 4 Dye from Wastewater Effluents. *J. Taiwan Inst. Chem. Eng.* **2021**, *125*, 141–152. [[CrossRef](#)]
57. Arun, G.; Ayoub, M.; Zulqarnain, Z.; Deshannavar, U.; Yusoff, M.H.M.; Farrukh, S.; Sher, F. Valorization of Solketal Synthesis from Sustainable Biodiesel Derived Glycerol Using Response Surface Methodology. *Catalysts* **2021**, *11*, 1537. [[CrossRef](#)]